AGU PUBLICATIONS

Geophysical Research Letters

RESEARCH LETTER
10.1002/2017GL073129

Special Section:
Early Results: Juno at Jupiter

Magnetosphere-ionosphere coupling at Jupiter: Expectations for Juno Perijove 1 from a steady state axisymmetric physical model

S. W. H. Cowley[1], G. Provan[1], E. J. Bunce[1], and J. D. Nichols[1]

[1]Department of Physics and Astronomy, University of Leicester, Leicester, UK

Key Points:
- A model of magnetosphere-ionosphere coupling at Jupiter benchmarked against auroral data is evaluated on the Juno Perijove 1 trajectory
- Expected plasma regimes on PJ1 include six near-planet encounters with middle magnetosphere (main oval) field lines at radii ~1.6 to ~16 R_J
- Field effects produced by expected distributed polar downward currents and main oval upward currents are quantified for comparison with data

Supporting Information:
- Supporting Information S1

Correspondence to:
S. W. H. Cowley,
swhc1@ion.le.ac.uk

Citation:
Cowley, S. W. H., G. Provan, E. J. Bunce, and J. D. Nichols (2017), Magnetosphere-ionosphere coupling at Jupiter: Expectations for Juno Perijove 1 from a steady state axisymmetric physical model, *Geophys. Res. Lett.*, *44*, doi:10.1002/2017GL073129.

Received 17 FEB 2017
Accepted 23 APR 2017

Abstract We evaluate the expected effects of magnetosphere-ionosphere coupling at Jupiter along the Juno Perijove 1 (PJ1) trajectory using an axisymmetric physical model. As found at Saturn, the model predicts distributed downward field-aligned currents over polar regions mapping to the tail and outer magnetosphere, closed principally through a ring of upward current mapping to the middle magnetosphere, which requires downward acceleration of magnetospheric electrons generating Jupiter's main auroral emission. Auroral location, width, intensity, electron energy, and current density are in accord with values derived from previous ultraviolet imaging, such that the model forms an appropriate baseline for comparison with Juno data. We evaluate the azimuthal field perturbations during six anticipated near-planet encounters with middle magnetosphere field lines at radial distances between ~1.6 and ~16 Jovian radii, discuss the expected form of the accelerated electron distributions, and comment briefly on model expectations in relation to first results derived from Juno PJ1 data.

1. Introduction

A primary goal of the Juno mission is to make the first measurements of particles, fields, and auroras directly over Jupiter's poles [*Bagenal et al.*, 2017]. Relevant instrumentation consists of two ion and electron spectrometers that together cover the energy range of ~100 eV to ~1 MeV, a magnetic field investigation capable of measuring fields up to ~1.6 mT, a wave experiment that detects plasma waves and radio emissions in the frequency range of 50 Hz to 40 MHz, and imaging spectrometers that remotely observe auroral emissions at both ultraviolet (UV) and infrared (IR) wavelengths [see *Connerney et al.*, 2017b, and references therein]. Prior to the arrival of Juno, detailed observations concerning magnetosphere-ionosphere coupling at Jupiter were available only from imaging of the polar aurora, both at UV wavelengths using the Hubble Space Telescope (HST) [e.g., *Clarke et al.*, 1998, 2009; *Pallier and Prangé*, 2001; *Grodent et al.*, 2003a, 2003b; *Nichols et al.*, 2009a, 2009b; *Gérard et al.*, 2013, 2014] and at IR wavelengths (ionospheric H_3^+ emissions) using ground-based telescopes [e.g., *Stallard et al.*, 2001, 2003, 2016]. Bright discrete auroras are believed to be associated with downward electron acceleration in the upward field-aligned components of the large-scale current systems that couple momentum between the ionosphere and magnetosphere [e.g., *Kennel and Coroniti*, 1975; *Cowley and Bunce*, 2001; *Hill*, 2001; *Bunce et al.*, 2004; *Nichols and Cowley*, 2004]. With increasing latitude in the ionosphere, these emissions consist of moon footprint auroras mapping along field lines to Io at 5.9 R_J, Europa at 9.4 R_J, and Ganymede at 15 R_J, the main oval emissions mapping equatorially beyond ~15 R_J, and structured variable polar emissions mapping variously to the cusp magnetopause on the dayside and into the far tail on the nightside [*Vogt et al.*, 2011, 2015]. (R_J is Jupiter's equatorial 1 bar radius equal to 71,492 km.)

The main emission, a focus of the present paper, is relatively steady in time and forms an oval around both poles which usually is nearly, but not completely, continuous in local time (LT) [*Radioti et al.*, 2008]. It has been proposed to be formed in a region of upward directed field-aligned current associated with the breakdown of near-rigid plasma corotation in the equatorial magnetosphere beyond ~15–20 R_J [*Cowley and Bunce*, 2001; *Hill*, 2001; *Nichols and Cowley*, 2004], as indicated both by auroral IR Doppler observations [e.g., *Stallard et al.*, 2001, 2003] and in situ equatorial plasma data [e.g., *Frank and Paterson*, 2002, 2004]. UV intensities determined from HST imaging are typically a few hundred kR, implying precipitating electron energy fluxes of a few tens of mW m^{-2} [e.g., *Grodent et al.*, 2003a; *Radioti et al.*, 2008; *Gérard et al.*, 2014]. Since the emission forms a ring of ~15° colatitude radius centered approximately on the magnetic poles, of width ~1.5°, the total main emission UV power is typically a few hundred GW, implying a total precipitating electron power of a few

TW [e.g., *Clarke et al.*, 2009; *Nichols et al.*, 2009a, 2017]. Observations of the UV spectrum further imply main emission electron primary energies of ~50–100 keV [e.g., *Gustin et al.*, 2004; *Gérard et al.*, 2014], such that with the above energy fluxes, the ionospheric upward directed current densities carried by these electrons are a few hundred nA m^{-2}, with a total azimuth-integrated upward current of several tens of MA per hemisphere.

A steady state axisymmetric physical model of magnetosphere-ionosphere coupling at Jupiter whose main emission region properties are compatible with the above data was constructed by *Cowley et al.* [2005], with further development by *Cowley et al.* [2008] allowing the coupling parameters at ionospheric heights to be projected along field lines to form a realistic model of associated magnetic perturbations in the magnetosphere. Although subsequently developed to include complications such as thermospheric coupling, nonaxisymmetry effects, and time-dependence [e.g., *Smith and Aylward*, 2009; *Tao et al.*, 2010; *Ray et al.*, 2014; *Chané et al.*, 2017], the underlying physics remains unchanged, such that the *Cowley et al.* [2005, 2008] model represents an appropriate theoretical baseline to compare with Juno data. In their discussion of initial results from the first science periapsis pass of Juno Perijove 1 (PJ1) in late August 2016, when all of the above mentioned instruments were fully operational, *Connerney et al.* [2017b] have indicated that identification of significant field-aligned current signatures on auroral field lines has remained elusive. A principal purpose of the present paper therefore is to quantify in detail the field-aligned current signatures and related auroral particle effects expected on the PJ1 trajectory on the basis of the *Cowley et al.* [2008] model, so that a clear comparison with expectations can subsequently be made. Although related results were presented previously by these authors evaluated on Juno planning orbits, the detailed nature of the expected field effects, i.e., their timing, and hence their radial distance and magnitude, and whether representing partial or complete crossings of auroral field lines, depends quite sensitively on the spacecraft trajectory. Specifically, it depends on the figure of the orbit (i.e., the radial distance of apoapsis for a fixed periapsis), the variable inclination of the line of apsides of the near-polar orbit to the equatorial plane, and the timing of the pass relative to the planetary rotation and hence orientation of the planetary magnetic axis. The Juno planning orbit used by *Cowley et al.* [2008] differs significantly from PJ1 in employing an apoapsis radius of 39 R_J compared with ~113 R_J for PJ1 (both with a periapsis radius of ~1.06 R_J), a midmission inclination of the line of apsides of 20° compared with ~4° for PJ1, and an arbitrarily assigned planetary rotation phase unspecified at that time. The expected spacecraft sampling of auroral-related field lines is then quite different on the two trajectories, as demonstrated explicitly in Text S1 and Figure S1 in the supporting information, such that while illustrative, the earlier results do not form an appropriate basis for detailed comparison with Juno PJ1 data. Here we thus present results obtained from evaluation of the *Cowley et al.* [2008] model along the Juno PJ1 trajectory as flown, which do form the basis for such a comparison. Brief comments on Juno instrument capabilities relative to model expectations are provided in Text S2.

2. Theoretical Model

We begin with brief details of the *Cowley et al.* [2005, 2008] model, a fuller description of which is provided in Text S3 and Figure S2. As indicated above, the primary assumptions of the model are that the system is steady state and axisymmetric about the magnetic axis, taken to be the dipole axis of the VIP4 model of *Connerney et al.* [1998], tilted by 9.515° to the planet's spin axis with the northern pole at azimuth 159.225° in right-hand System III. All the fields discussed here are spherical polar components referenced to this axis. The essential physics of the model is contained in the angular velocity profile of the ionospheric plasma $\omega_i(\theta_i)$ around this axis, varying with colatitude θ_i at radius $R_i \approx 67,350$ km, relative to that of the planet ($\Omega_J \approx 1.7585 \times 10^{-4}$ rad s^{-1}corresponding to a rotation period of ~9.925 h). Four regions are identified based on empirical data and prior theoretical modeling (Figure S2), which from pole to equator are (a) tail field lines mapping beyond ~150 R_J where the plasma is strongly subcorotational with $\omega_i/\Omega_J = 0.1$, (b) outer magnetosphere field lines mapping to the "cushion region" on the dayside where the angular velocity increases to $\omega_i/\Omega_J = 0.35$, (c) middle magnetosphere field lines mapping equatorially to the magnetodisk between ~15 and ~50 R_J across which the angular velocity increases sharply toward rigid corotation, and (d) the inner quasi-dipolar magnetosphere mapping inside ~15 R_J where the plasma near-rigidly corotates $\omega_i/\Omega_J \approx 1$ (Figure S2a). In the figures these regions are color-coded blue, yellow, red, and white, respectively.

The electric field of the ionospheric flow relative to the neutral atmosphere drives an equatorward Pedersen current in both hemispheres, which increases from zero at the poles to peak at an azimuth-integrated value of ~54 MA near the outer-middle magnetosphere boundary and falls to zero across the middle magnetosphere layer as the angular velocity rises toward rigid corotation (Figure S2b). Current continuity then requires distributed downward field-aligned current densities at ionospheric height $j_{||i}$ of ~55–80 nA m^{-2} to flow into the ionosphere on tail and outer magnetosphere field lines where the integrated equatorward current rises with colatitude from the poles, while an upward current peaking at ~400 nA m^{-2} flows out of the middle magnetosphere layer where it falls (Figure S2c). These currents extend along field lines with $(j_{||}/B) = \text{constant}$, closing across the field at large distances in the equatorial magnetosphere and magnetopause. From Ampère's law these currents generate an azimuthal field B_ϕ, pervading the subcorotating magnetosphere, negative north and positive south, reversing sign across the equatorial closure currents, such that field lines are bent out of magnetic meridians into a "lagging" or "sweepback" configuration. Just above the ionosphere the model field $B_{\phi i}$ increases from zero at the pole to peak at ~620 nT near the outer-middle magnetosphere boundary, and then falls to zero across the middle magnetosphere layer (Figure S2d). Ampère's law further shows that B_ϕ varies along each field line as $B_\phi = B_{\phi i}(\rho_i/\rho)$ between the ionospheric and magnetospheric closure currents, where ρ is perpendicular distance from the magnetic axis.

Based on equatorial Voyager data, *Cowley et al.* [2008] estimated that the maximum upward current density that can be carried by hot ($W_{th} \approx 2.5$ keV) plasma sheet electrons precipitating into the ionosphere on middle magnetosphere field lines, corresponding to a full downward and empty upward loss cone, is $j_{||i0} \approx 15$ nA m^{-2} (Text S3). Since the required peak upward current on these field lines exceeds this by a factor of ~30, downward electron acceleration is required. Acceleration parameters are estimated using the kinetic theory of *Knight* [1973], who showed that the minimum field-aligned voltage is $\Phi_{||\min} = (W_{th}/e)((j_{||i}/j_{||i0}) - 1)$ assuming acceleration well above the minimum radial distance $r_{\min} \approx R_i(j_{||i}/j_{||i0})^{1/3}$, at which point all the downward moving electrons need to be accelerated into the ionosphere to carry the current, then requiring an infinite voltage. In a dipole field, the required voltage falls close to the minimum value if the acceleration region lies beyond approximately twice the minimum distance [e.g., *Cowley and Bunce*, 2001]. The corresponding precipitating energy flux is $E_{fi} = (E_{f\ i0}/2)((j_{||i}/j_{||i0})^2 + 1)$, where $E_{f\ i0}$ is the unaccelerated value similarly estimated to be ~0.1 mW m^{-2}. Significant model field-aligned voltages thus occur across most of the middle magnetosphere layer, with peak values near the center of ~80 kV, forming an "inverted V" electron precipitation pattern across the feet of middle magnetosphere field lines (Text S3 and Figure S2e). The peak model precipitating energy flux is ~35 mW m^{-2} sufficient to excite UV auroras of ~350 kR (Figure S2f), compared with ~1 kR for the unaccelerated population. These values, together with the colatitude and width, are comparable with UV observations discussed in section 1, such that the model provides an appropriate baseline for comparison with Juno data. The model also indicates that the acceleration region must lie above ~3 R_J (Figure S2h), with the accelerating voltages thus falling close to minimum values for locations above ~6 R_J.

Directly beneath the acceleration region the electrons form a near monoenergetic downgoing beam of angular pitch angle extent $\alpha_b \approx (W_{th}/e\Phi_{||\min})^{1/2} \approx (j_{||i0}/j_{||i})^{1/2}$ about the field direction, assuming the minimum field-aligned voltage applies [e.g., *Paschmann et al.*, 2003, section 3.3]. This angle is ~10° for $(j_{||i}/j_{||i0}) \approx 30$ at the peak of the middle magnetosphere current layer, such that the electron beam is highly collimated about the field direction. In the absence of strong scattering a mirrored upgoing beam is also present, such that the distribution is bidirectional, with a narrow loss cone in the upgoing population giving the net downward electron flux and upward directed current. At larger distances below the acceleration region, however, mirroring causes both beams to widen in pitch angle toward a spherical shell, again with a widening loss cone in the upward directed population. In a dipole field the spherical shell will be approximately fully formed at radial distances $r \approx r_{\text{acc}}(j_{||i0}/j_{||i})^{1/3}$, where r_{acc} is the radial distance of the acceleration region. Taking this radius to be an (essentially unknown) factor f larger than the minimum value, $r_{\text{acc}} \approx fr_{\min}$, the shell distribution will be near fully formed below radius $r \approx fR_i$. Such shell-loss cone distributions are known to be subject to cyclotron maser instability [e.g., *Paschmann et al.*, 2003, section 4.3; *Mutel et al.*, 2010], giving rise to intense auroral radio emissions close to the local electron cyclotron frequency in the source region and leading to strong electron diffusion in velocity space. This process gives rise to both terrestrial auroral kilometric radiation (AKR) and

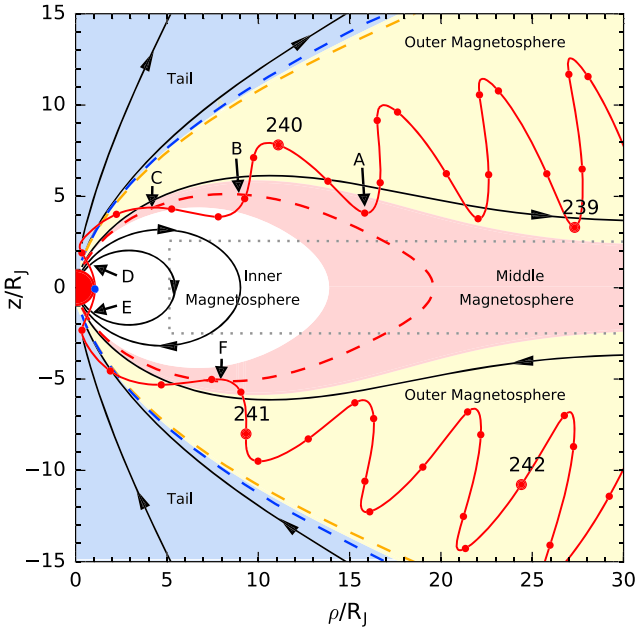

Figure 1. PJ1 trajectory (red) projected into a magnetic meridian in cylindrical (ρ, z) coordinates (R_J). The large red circles show the start of each day marked with DOY 2016, the small red circles are plotted every 2 h, and the blue circle shows periapsis. The black lines show model field lines mapping to the ionosphere at intervals of 5° colatitude between the pole and 25°, the field being the sum of the VIP4 dipole and that due to an annular ring current flowing in the equatorial rectangle outlined by gray dots. The blue, yellow, red, and white areas indicates tail, outer, middle, and inner magnetosphere field lines, respectively, with the blue and yellow dashed lines indicating the upward current layer at the tail field boundary, and the red dashed line the field-aligned current density peak on middle magnetosphere field lines. The arrows labeled A–F indicate the positions of six anticipated near-planet Juno encounters with middle magnetosphere field lines.

Saturn kilometric radiation (SKR) in upward directed current regions and may thus provide an additional indicator of downward electron acceleration in upward directed current regions at Jupiter.

3. Juno PJ1 Trajectory

During the PJ1 pass the Juno orbit was located close to Jupiter's dawn-dusk meridian, with apoapsis at ~113 R_J ~3.3° south of the equator at dawn and periapsis at ~1.06 R_J ~3.8° north of the equator at dusk. Figure 1 shows the trajectory (red) over an ~3 day interval projected into a magnetic meridian in the region $0 \le \rho \le 30$ R_J and $-15 \le z \le 15$ R_J, z being distance from the magnetic equator. Periapsis is marked with the blue circle, with larger red circles indicating the start of day labeled with day of year (DOY) 2016 and smaller red circles being plotted at 2 h intervals. The model field consists of the VIP4 planetary dipole, plus the field of a ring current which stretches the equatorial field into a magnetodisk forming the middle magnetosphere. The ring current is based on the *Connerney et al.* [1981] model, where the azimuthal current density falls as $j_\phi = I_o/\rho$ within an annular disk of half-width D about the magnetic equator between cylindrical radii R_1 and R_2 and is zero elsewhere. The parameters employed are $D = 2.5$ R_J, $R_1 = 5.25$ R_J, and $R_2 = 60$ R_J, outlined by the gray dotted box in Figure 1, together with $\mu_o I_o = 350$ nT, though the results are not sensitively dependent on these choices. The model field lines (black), obtained by contouring the flux function [*Edwards et al.*, 2001], intersect the ionosphere at 5° intervals between 0° mapping to the tail and 25° mapping equatorially to ~5.3 R_J close to the ring current inner edge. As indicated in section 2, the blue, yellow, and red areas show tail, outer, and middle magnetosphere (magnetodisk) field lines, respectively, while the red dashed line indicates the maximum upward current density flowing in the middle magnetosphere, closing via an outward radial current within the ring current disk. The white area shows the inner magnetosphere where near-corotating quasi-dipolar flux tubes contain trapped energetic particles.

Figure 1 shows that during approach to and recession from the planet Juno is anticipated to have been located principally on northern and southern outer magnetosphere field lines, respectively. However, during an ~1 day interval centered near periapsis, Juno is expected to have made six near-planet encounters with middle magnetosphere (main emission) field lines, labeled A–F. The first three occur inbound with the spacecraft located near the dawn meridian, consisting of a partial entry from the outer magnetosphere centered at ~16.2 R_J (A), a full crossing of the middle magnetosphere layer into the inner magnetosphere at ~10.4 R_J (B), and a full reverse transition at ~6.4 R_J (C). The spacecraft then passes onto tail field lines at ~3.9 R_J in the dawn sector before traversing the planetary pole into the dusk sector. It then moves equatorward back across the tail field boundary at ~1.8 R_J, followed by a rapid crossing of middle magnetosphere field lines at ~1.6 R_J (D) into the inner magnetosphere, and then a reversed sequence of transitions in the southern hemisphere

across the middle magnetosphere layer at ~1.7 R_J (E) and tail boundary at ~1.9 R_J in the dusk sector. It then once more traverses the pole and crosses the tail boundary onto southern outer magnetosphere field lines in the dawn sector at ~5.4 R_J. One further partial crossing onto middle magnetosphere field lines follows at ~9.3 R_J (F). Thus six near-planet encounters with middle magnetosphere field lines are anticipated to have taken place at radii between ~1.6 and ~16.2 R_J.

4. Model Parameters on the PJ1 Trajectory

Figure 2 shows model parameters evaluated versus time on the PJ1 trajectory. Figures 2a–2e show a 2 day interval centered near periapsis (vertical dashed line), from 12 h on DOY 239 to 12 h on DOY 241. Figure 2 a shows the spacecraft mapped ionospheric colatitude θ_i (relative to either pole), with blue and red indicating a location north or south of the equator, respectively. The horizontal dotted lines indicate the magnetospheric regimes to which the field lines map, with vertical blue, yellow, red, and white bars indicating locations on model tail, outer, middle, and inner magnetosphere field lines, respectively, as in Figures 1 and S2. The six encounters with middle magnetosphere field lines are labeled A–F as in Figure 1. Figure 2b shows the model normalized plasma angular velocity. Figure 2c shows the model poloidal fields on a log scale, where the black line shows B_θ (everywhere positive); the red and blue lines the magnitude of B_r in regions where it is positive and negative, respectively; and the dotted line the total poloidal field strength. Figure 2d shows the field-aligned current density at the spacecraft on a log scale, where the red and blue lines indicate upward and downward currents, respectively, relative to the spacecraft's hemisphere. Figure 2e shows the associated sweepback field B_ϕ on a scale appropriate to the outer regions. Figures 2f–2h show parameters on an expanded time scale for the close-periapsis pass, specifically the interval 9.5–17.5 h UT on DOY 240, during which Juno traversed both northern and southern tail field regions (blue) between dawn and dusk via a near-periapsis equator crossing in the dusk sector. Figure 2f shows the field-aligned current density at the spacecraft in the same format as Figure 2d (though with a revised range), Figure 2g shows the sweepback field on a scale appropriate to the inner region, while Figure 2h shows the minimum radial distance of the auroral electron acceleration regions together with the radial distance of the spacecraft (dotted line).

We first note that comparison of Figure 2 with the Juno data for day 240 discussed by *Connerney et al.* [2017b] shows good overall correspondence with the plasma regimes observed. A dip occurs into the radiation belt (inner magnetosphere shown white in Figure 2) between ~4 and ~8 UT as expected, with subsequent few-hour traversals of northern and southern polar field lines either side of the near-periapsis interval (outer magnetosphere and tail regions shown yellow and blue), and indications in particle and wave data of crossings of auroral field lines in the vicinity of each of the anticipated day 240 middle magnetosphere field line encounters B–F (red, with two crossings in interval F since the trajectory passed twice across the center of the model layer). While the latter regions are anticipated to correspond to intervals of upward field-aligned current, Figure 2f shows that during the near-periapsis interval the spacecraft is expected mostly to have been immersed in regions of weaker downward field-aligned current. This follows from the overall nature of the model current system (Figure S2) where distributed downward currents flow over broad subcorotating polar regions mapping to the tail and outer magnetosphere. Correspondingly, *Connerney et al.* [2017b] report that upwardly directed field-aligned electron beams indicative of downward currents, or sometimes asymmetric bidirectional beams, broadly spread in energy between tens to hundreds of keV, are a pervasive feature of the polar PJ1 data in regions identified in Figure 2 as tail or outer magnetosphere. Similar conditions apply also at Saturn where the planetary field has the same polarity relative to the planetary spin, where magnetic field data show directly that distributed downward currents flow over the polar region, closed by a ring of upward current mapping to the auroral oval located just equatorward of the tail field boundary [*Hunt et al.*, 2014, 2015]. These downward current regions are also associated with upward accelerated electron beams, and with light ion conics, with energies ~100 keV [e.g., *Mitchell et al.*, 2009].

We now focus on middle magnetosphere (main emission) field lines, where upward directed field-aligned currents are expected to switch off the sweepback field pervading the subcorotating magnetosphere between the outer and inner magnetosphere regions, leading to clear expected azimuthal field signatures during layer encounters A–F as shown in Figures 2e and 2g. Encounter A represents a partial penetration of middle magnetosphere field lines from and to the outer magnetosphere centered at ~20 h UT on DOY 239 at a radial distance of ~16.2 R_J, though the trajectory does not reach the center of the layer. Due to

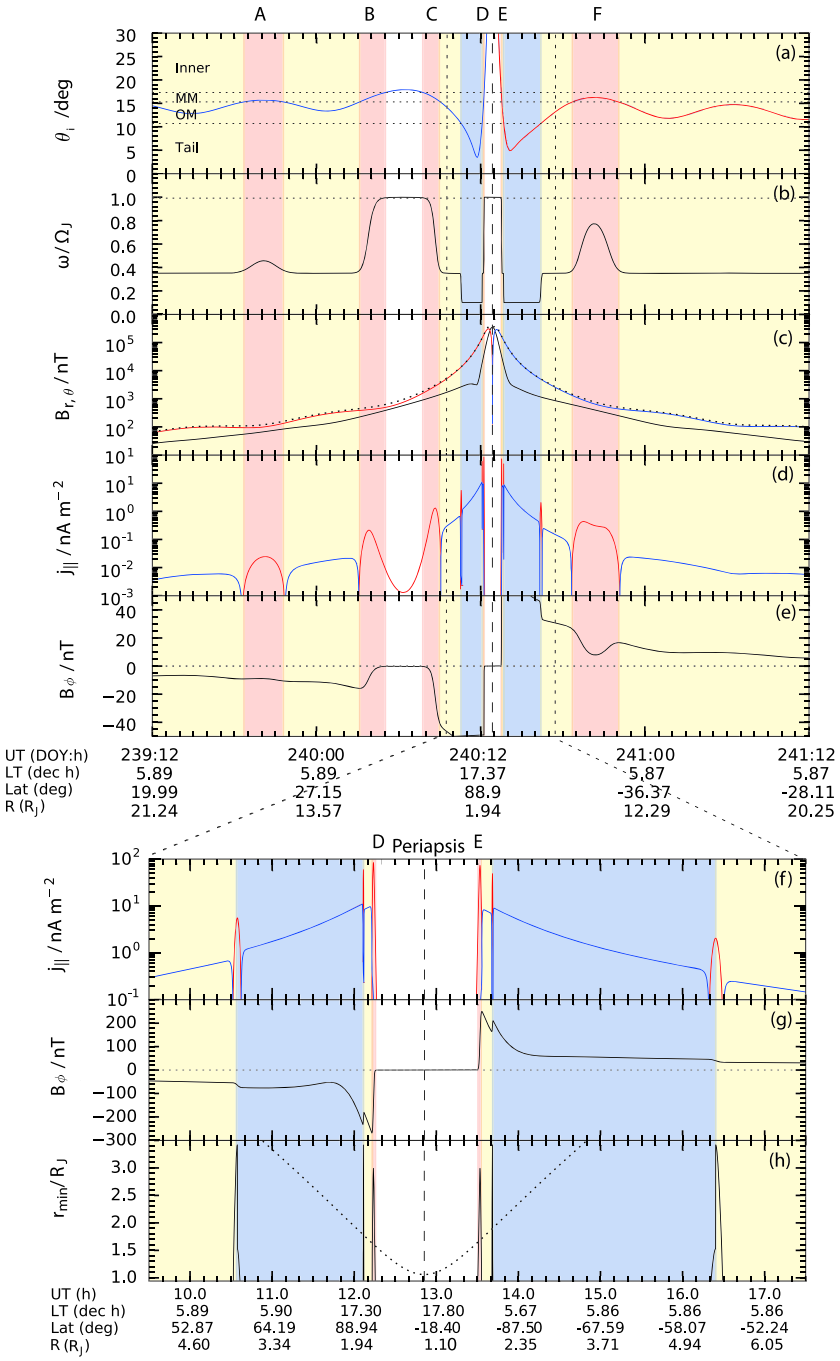

Figure 2. Model parameters versus time evaluated on the PJ1 trajectory. A 2 day interval from 12 h UT on DOY 239 to 12 h UT on DOY 241 centered near periapsis (vertical dashed line) showing (a) mapped spacecraft ionospheric colatitude θ_i (deg) with region identifiers as in Figure 1; (b) normalized plasma angular velocity (ω/Ω_J); (c) poloidal field components (nT) on a log scale, B_θ black (everywhere positive), B_r red and blue corresponding to positive and negative, respectively, and total poloidal field strength (dotted); (d) $j_{||}$ (nA m^{-2}) local to the spacecraft on a log scale, red and blue corresponding to positive (upward) and negative (downward), respectively; and (e) sweepback field B_ϕ (nT) on a scale appropriate to the outer regions. The interval from 9.5 to 17.5 h UT on DOY 240 showing (f) $j_{||}$ (nA m^{-2}) in the same format as Figure 2d (note change in range), (g) sweepback field B_ϕ (nT) on a scale appropriate to the inner region, and (h) minimum radius of the electron acceleration region r_{min} (R_J) in upward current regions, together with the spacecraft radial distance (dotted line). The colored bars indicate physical regimes as in Figure 1. Data beneath each set of panels give the time (UT), together with the LT (hours), latitude (deg), and radial distance (R_J) of the spacecraft.

both the distance and the partial penetration, the B_ϕ perturbations in Figure 2e are muted, consisting of an ~1.5 nT increase from ~ −10 nT to smaller negative values and back over an ~2.5 h interval. This change is superposed on an expected poloidal field of ~100 nT (Figure 2c). Encounter B, however, corresponds to a full crossing of the middle magnetosphere layer from outer to inner magnetosphere field lines centered at ~04 h UT on DOY 240 at ~10.4 R_J, across which model B_ϕ increases from −16 nT to near-zero values over an ~1.5 h interval, superposed on a planetary field of ~500 nT. At encounter C at ~08:30 h UT and ~6.4 R_J, the PJ1 trajectory then crosses back from inner to outer magnetosphere field lines, such that B_ϕ decreases again from near-zero to ~ −40 nT over an ~1 h interval, in a planetary field of ~2500 nT. These B_ϕ variations are the near-planet signatures of the upward field-aligned currents anticipated to drive the main auroral emissions. Encounter F on the dawnside outbound pass centered at ~20:30 h UT on DOY 240 at ~9.3 R_J has a similar character. An extended partial penetration of middle magnetosphere field lines takes place from and to outer magnetosphere field lines, which now passes twice across the center of the model layer as noted above, resulting in a reduction in B_ϕ from ~ +26 to ~ +8 nT over an initial ~1 h interval, followed by a return to ~ +17 nT over a subsequent ~1.5 h interval, in a planetary field of ~750 nT. We note that all of these encounters take place at radii well above the minimum radial distance of the auroral acceleration region ~3 R_J (Figure S2h), though only by a factor of ~2 for encounter C.

During the close periapsis pass shown in Figures 2f–2h the near-periapsis encounters with middle magnetosphere field lines in the dusk sector occur at ~12:14 UT in the north (D) and ~13:32 UT in the south (E), respectively, resulting in rapid reductions in the magnitude of B_ϕ from ~255 nT on the outer magnetosphere side of the layer to near-zero in the inner magnetosphere, each occurring over ~2 min in a planetary field of ~200,000 nT. We emphasize, however, that the near-planet azimuthal fields associated with magnetosphere-ionosphere coupling calculated here will in general be superposed on planetary azimuthal fields of comparable or larger magnitude not described by our axisymmetric model. However, since the planetary field will generally vary relatively smoothly in space, the auroral effects should be readily distinguishable through the sharp changes occurring across the field-aligned current layers whose expected position, magnitude, and duration on PJ1 are as shown in Figure 2.

Since encounters D and E take place at radii of ~1.6 and ~1.7 R_J, respectively, well below the ~3 R_J minimum for the acceleration region (Figure S2h), Juno is expected to pass beneath the acceleration regions at least in these cases, briefly observing the downward accelerated electrons responsible for the main emissions, whose anticipated properties were outlined in section 2. As indicated above, however, the polar Juno particle measurements reported by *Connerney et al.* [2017b] instead emphasize upward accelerated electron beams or asymmetric bidirectional beams with broad energy spectra, more indicative of downward directed currents. Nevertheless, we note that at each of the anticipated Juno encounters with middle magnetosphere field lines B–F on day 240 (data were not shown for interval A on day 239), intense radio emissions were observed at or just above the local electron cyclotron frequency (twice for encounter F as noted above), indicative of proximity to AKR/SKR-type radio emission source regions at radii out to ~11 R_J [*Connerney et al.*, 2017b]. As noted in section 2, such emissions are potentially indicative of shell-loss cone electron distributions formed in downward directed acceleration regions located well above the minimum radius. Further study of accelerated particle properties in conjunction with wave and field data is thus called for. We note in this context that Cassini has yet routinely to fly at sufficiently low altitudes across auroral field lines at Saturn to observe the expected downward accelerated primary auroral electrons in the observed ring of upward current surrounding the polar distributed downward currents, anticipated from theory and UV data in this case to be of ~10 keV energy [e.g., *Cowley et al.*, 2004; *Gérard et al.*, 2009].

5. Summary

We have calculated expected effects of Jupiter's magnetosphere-ionosphere coupling in Juno PJ1 data by evaluating a steady state axisymmetric physical model along the spacecraft trajectory and have commented briefly on the results in relation to the initial discussion of PJ1 data by *Connerney et al.* [2017b]. Due to the common polarity of the planetary field and spin axes, the coupling currents at Jupiter are expected to have the same basic form as observed by Cassini at Saturn, with distributed downward currents over wide subcorotating polar regions mapping to the tail and outer magnetosphere, closed by one or more narrower rings of more intense upward current where the plasma angular velocity increases toward corotation. The

expectation of distributed downward currents at polar latitudes appears compatible with Juno observations of extended intervals of upward directed electron acceleration in the northern and southern polar regions, taking the form of upward field-aligned or asymmetric bidirectional electron beams. The dominant upward current at Jupiter is expected to flow on middle magnetosphere field lines mapping to the magnetodisk in the equatorial magnetosphere (~15–50 R_J) and to the main emission region in the polar ionosphere, separating the subcorotating region where an azimuthal sweepback field is present from the inner near-corotating magnetosphere where it is not. The expected azimuthal field perturbations during six anticipated PJ1 encounters with the middle magnetosphere upward directed current layer have been evaluated, two of which occur at radii of ~1.6 R_J at dusk, and four at distances between ~6 and 16 R_J at dawn, these field lines being the potential locations of downward field-aligned electron acceleration whose expected nature has been outlined. While auroral-related signatures were reported by *Connerney et al.* [2017b] during five of the six anticipated middle magnetosphere field line encounters (the data they discussed did not cover encounter A at greatest distances), in particular, intense radio emissions near the electron cyclotron frequency potentially indicative of the cyclotron maser instability and downward electron acceleration, direct identification of expected signatures of upward directed currents in particle, and field data have proven to be elusive. Detailed studies of PJ1 (and subsequent Juno perijove) data in relation to the detailed model expectations reported in this paper are clearly warranted.

Acknowledgments
Work at the University of Leicester was supported by STFC Consolidate Grant ST/N000749/1. We thank the Juno Science Operations Center team at SwRI for access to Juno trajectory data. Model data for PJ1 and other passes are available from the authors on request.

References

Acuña, M. H., K. W. Behannon, and J. E. P. Connerney (1983), Jupiter's magnetic field and magnetosphere, in *Physics of the Jovian Magnetosphere*, edited by A. J. Dessler, pp. 1–50, Cambridge Univ. Press, Cambridge, U. K.

Badman, S. V., and S. W. H. Cowley (2007), Significance of Dungey cycle flows in Jupiter's and Saturn's magnetospheres, and their identification on closed equatorial field lines, *Ann. Geophys.*, *25*, 941–951.

Bagenal, F., et al. (2017), Magnetospheric science objectives of the Juno mission, *Space Sci. Rev.*, 1–69, doi:10.1007/s11214-014-0036-8.

Bunce, E. J., S. W. H. Cowley, and T. K. Yeoman (2004), Jovian cusp processes: Implications for the polar aurora, *J. Geophys. Res.*, *109*, A09S13, doi:10.1029/2003JA010280.

Chané, E., J. Saur, R. Keppens, and S. Poedts (2017), How is the jovian main emission affected by the solar wind?, *J. Geophys. Res. Space Physics*, *122*, 1960–1978, doi:10.1002/2016JA023218.

Clarke, J. T., et al. (1998), Hubble Space Telescope imaging of Jupiter's UV aurora during the Galileo orbiter mission, *J. Geophys. Res.*, *103*, 20,217–20,236, doi:10.1029/98JE01130.

Clarke, J. T., et al. (2009), The response of Jupiter's and Saturn's auroral activity to the solar wind, *J. Geophys. Res.*, *114*, A05210, doi:10.1029/2008JA013694.

Connerney, J. E. P., M. H. Acuña, and N. F. Ness (1981), Modeling the jovian current sheet and inner magnetosphere, *J. Geophys. Res.*, *86*, 8370–8384, doi:10.1029/JA086iA10p08370.

Connerney, J. E. P., M. H. Acuña, N. F. Ness, and T. Satoh (1998), New models of Jupiter's magnetic field constrained by the Io flux tube footprint, *J. Geophys. Res.*, *103*, 11,929–11,940, doi:10.1029/97JA03726.

Connerney, J. E. P., et al. (2017a), The Juno magnetic field investigation, *Space Sci. Rev.*, doi:10.1007/s11214-017-0334-z, in press.

Connerney, J. E. P., et al. (2017b), Jupiter's magnetosphere and aurorae observed by the Juno spacecraft during its first polar orbits, *Science*, doi:10.1126/science.aam5928, in press.

Cowley, S. W. H., and E. J. Bunce (2001), Origin of the main auroral oval in Jupiter's coupled magnetosphere-ionosphere system, *Planet. Space Sci.*, *49*, 1067–1088.

Cowley, S. W. H., E. J. Bunce, and J. M. O'Rourke (2004), A simple quantitative model of plasma flows and currents in Saturn's polar ionosphere, *J. Geophys. Res.*, *109*, A05212, doi:10.1029/2003JA010375.

Cowley, S. W. H., I. I. Alexeev, E. S. Belenkaya, E. J. Bunce, C. E. Cottis, V. V. Kalegaev, J. D. Nichols, R. Prangé, and F. J. Wilson (2005), A simple axi-symmetric model of magnetosphere-ionosphere coupling currents in Jupiter's polar ionosphere, *J. Geophys. Res.*, *110*, A11209, doi:10.1029/2005JA011237.

Cowley, S. W. H., A. S. Deason, and E. J. Bunce (2008), Axisymmetric model of auroral current systems in Jupiter's magnetosphere with predictions for the Juno mission, *Ann. Geophys.*, *26*, 4051–4074.

Edwards, T. M., E. J. Bunce, and S. W. H. Cowley (2001), A note on the vector potential of Connerney et al.'s model of the equatorial current sheet in Jupiter's magnetosphere, *Planet. Space Sci.*, *49*, 1115–1123.

Frank, L. A., and W. R. Paterson (2002), Galileo observations of electron beams and thermal ions in Jupiter's magnetosphere and their relation to the auroras, *J. Geophys. Res.*, *107*(A12), 1478, doi:10.1029/2001JA009150.

Frank, L. A., and W. R. Paterson (2004), Plasmas observed near local noon in Jupiter's magnetosphere with the Galileo spacecraft, *J. Geophys. Res.*, *109*, A11217, doi:10.1029/2002JA009795.

Gérard, J.-C., B. Bonfond, J. Gustin, D. Grodent, J. T. Clarke, D. Bisikalo, and V. I. Shematovich (2009), Altitude of Saturn's aurora and its implications for the characteristic energy of precipitated electrons, *Geophys. Res. Lett.*, *36*, L02202, doi:10.1029/2008GL036554.

Gérard, J.-C., D. Grodent, A. Radioti, B. Bonfond, and J. T. Clarke (2013), Hubble observations of Jupiter's north-south conjugate ultraviolet aurora, *Icarus*, *226*, 1559–1567.

Gérard, J.-C., B. Bonfond, D. Grodent, A. Radioti, J. T. Clarke, G. R. Gladstone, J. H. Waite, D. Bisikalo, and V. I. Shematovich (2014), Mapping the electron energy in Jupiter's aurora: Hubble spectral observations, *J. Geophys. Res. Space Physics*, *119*, 9072–9088, doi:10.1002/2014JA020514.

Grodent, D., J. T. Clarke, J. Kim, J. H. Waite, Jr., and S. W. H. Cowley (2003a), Jupiter's main oval observed with HST-STIS, *J. Geophys. Res.*, *108*(A11), 1389, doi:10.1029/2003JA009921.

Grodent, D., J. T. Clarke, J. H. Waite, Jr., S. W. H. Cowley, and J. Kim (2003b), Jupiter's polar auroral emissions, *J. Geophys. Res.*, *108*(A10), 1366, doi:10.1029/2003JA010017.

Gustin, J., J.-C. Gérard, D. Grodent, S. W. H. Cowley, J. T. Clarke, and A. Grard (2004), Energy-flux relationship in the FUV jovian aurora deduced from HST-STIS spectral observations, *J. Geophys. Res.*, *109*, A10205, doi:10.1029/2003JA010365.

Hess, S. L. G., B. Bonfond, P. Zarka, and D. Grodent (2011), Model of the Jovian magnetic field topology constrained by the Io auroral emissions, *J. Geophys. Res.*, *116*, A05217, doi:10.1029/2010JA016262.

Hill, T. W. (1979), Inertial limit on corotation, *J. Geophys. Res.*, *84*, 6554–6558, doi:10.1029/JA084iA11p06554.

Hill, T. W. (2001), The jovian auroral oval, *J. Geophys. Res.*, *106*, 8101–8107, doi:10.1029/2000JA000302.

Hunt, G. J., S. W. H. Cowley, G. Provan, E. J. Bunce, I. I. Alexeev, E. S. Belenkaya, V. V. Kalegaev, M. K. Dougherty, and A. J. Coates (2014), Field-aligned currents in Saturn's southern nightside magnetosphere: Sub-corotation and planetary period oscillation components, *J. Geophys. Res. Space Physics*, *119*, 9847–9899, doi:10.1002/2014JA020506.

Hunt, G. J., S. W. H. Cowley, G. Provan, E. J. Bunce, I. I. Alexeev, E. S. Belenkaya, V. V. Kalegaev, M. K. Dougherty, and A. J. Coates (2015), Field-aligned currents in Saturn's northern nightside magnetosphere: Evidence for inter-hemispheric current flow associated with planetary period oscillations, *J. Geophys. Res. Space Physics*, *120*, 7552–7584, doi:10.1002/2015JA021454.

Isbell, J., A. J. Dessler, and J. H. Waite Jr. (1984), Magnetospheric energization by interaction between planetary spin and the solar wind, *J. Geophys. Res.*, *89*, 10,716–10,722, doi:10.1029/JA089iA12p10716.

Kane, M., B. H. Mauk, E. P. Keath, and S. M. Krimigis (1995), Hot ions in Jupiter's magnetodisc: A model for Voyager-2 low-energy charged particle measurements, *J. Geophys. Res.*, *100*, 19,473–19,486, doi:10.1029/95JA00793.

Kennel, C. F., and F. V. Coroniti (1975), Is Jupiter's magnetosphere like a pulsar's or Earth's?, *Space Sci. Rev.*, *17*, 857–883.

Knight, S. (1973), Parallel electric fields, *Planet. Space Sci.*, *21*, 741–750.

Krupp, N., A. Lagg, S. Livi, B. Wilken, J. Woch, E.C. Roelof, and D. J. Williams (2001), Global flows of energetic ions in Jupiter's equatorial plane: First-order approximation, *J. Geophys. Res.*, *106*, 26,017–26,032, doi:10.1029/2000JA900138.

Millward, G., S. Miller, T. Stallard, A. D. Aylward, and N. Achilleos (2002), On the dynamics of the jovian ionosphere and thermosphere III. The modelling of auroral conductivity, *Icarus*, *160*, 95–107.

Mitchell, D. G., W. S. Kurth, G. B. Hospodarsky, N. Krupp, J. Saur, B. H. Mauk, J. F. Carbary, S. M. Krimigis, M. K. Dougherty, and D. C. Hamilton (2009), Ion conics and electron beams associated with auroral processes at Saturn, *J. Geophys. Res.*, *114*, A02212, doi:10.1029/2008JA013621.

Mutel, R. L., J. D. Menietti, D. A. Gurnett, W. Kurth, P. Schippers, C. Lynch, L. Lamy, C. Arridge, and B. Cecconi (2010), CMI growth rates for Saturn kilometric radiation, *Geophys. Res. Lett.*, *37*, L19105, doi:10.1029/2010GL044940.

Nichols, J. D., and S. W. H. Cowley (2004), Magnetosphere-ionosphere coupling currents in Jupiter's middle magnetosphere: Effect of precipitation-induced enhancement of the ionospheric Pedersen conductivity, *Ann. Geophys.*, *22*, 1799–1827.

Nichols, J. D., J. T. Clarke, J. C. Gérard, D. Grodent, and K. C. Hansen (2009a), Variation of different components of Jupiter's auroral emission, *J. Geophys. Res.*, *114*, A06210, doi:10.1029/2008JA014051.

Nichols, J. D., J. T. Clarke, J. C. Gérard, and D. Grodent (2009b), Observation of Jovian polar auroral filaments, *Geophys. Res. Lett.*, *36*, L08101, doi:10.1029/2009GL037578.

Nichols, J. D., et al. (2017), Response of Jupiter's auroras to conditions in the interplanetary medium as measured by the Hubble Space Telescope and Juno, *Geophys. Res. Lett.*, doi:10.1002/2017GL073029, in press.

Pallier, L., and R. Prangé (2001), More about the structure of the high latitude Jovian aurorae, *Planet. Space Sci.*, *49*, 1159–1173.

Paschmann, G., S. Haaland, and R. Treumann (2003), Auroral plasma physics, *Space Sci. Rev.*, *103*, 1–475.

Radioti, A., J. C. Gérard, D. Grodent, B. Bonfond, N. Krupp, and J. Woch (2008), Discontinuity in Jupiter's main auroral oval, *J. Geophys. Res.*, *113*, A01215, doi:10.1029/2007JA012610.

Ray, L. C., N. A. Achilleos, M. F. Vogt, and J. N. Yates (2014), Local time variations in Jupiter's magnetosphere-ionosphere coupling system, *J. Geophys. Res. Space Physics*, *119*, 4740–4751, doi:10.1002/2014JA019941.

Scudder, J. D., E. C. Sittler Jr., and H. S. Bridge (1981), A survey of the plasma electron environment of Jupiter: A view from Voyager, *J. Geophys. Res.*, *86*, 8157–8179, doi:10.1029/JA086iA10p08157.

Smith, C. G. A., and A. D. Aylward (2009), Coupled rotational dynamics of Jupiter's thermosphere and magnetosphere, *Ann. Geophys.*, *27*, 199–230.

Stallard, T. S., S. Miller, G. Millward, and R. D. Joseph (2001), On the dynamics of the Jovian ionosphere and thermosphere: Part I. The measurement of ion winds, *Icarus*, 475–491.

Stallard, T. S., S. Miller, S. W. H. Cowley, and E. J. Bunce (2003), Jupiter's polar ionospheric flows: Measured intensity and velocity variations poleward of the main auroral oval, *Geophys. Res. Lett.*, *30*(5), 1221, doi:10.1029/2002GL016031.

Stallard, T. S., J. T. Clarke, H. Melin, S. Miller, J. D. Nichols, J. O'Donoghue, R. E. Johnson, J. E. P. Connerney, T. Satoh, and M. Perry (2016), Stability within Jupiter's polar auroral "swirl region" over moderate timescales, *Icarus*, *268*, 145–155.

Tao, C., H. Fujiwara, and Y. Kasaba (2010), Jovian magnetosphere–ionosphere current system characterized by diurnal variation of ionospheric conductance, *Planet. Space Sci.*, *58*, 351–364, doi:10.1016/j.pss.2009.10.005.

Vogt, M. F., M. G. Kivelson, K. K. Khurana, R. J. Walker, B. Bonfond, D. Grodent, and A. Radioti (2011), Improved mapping of Jupiter's auroral features to magnetospheric sources, *J. Geophys. Res.*, *116*, A03220, doi:10.1029/2010JA016148.

Vogt, M. F., E. J. Bunce, M. G. Kivelson, K. K. Khurana, R. J. Walker, A. Radioti, B. Bonfond, and D. Grodent (2015), Magnetosphere-ionosphere mapping at Jupiter: Quantifying the effects of using different internal field models, *J. Geophys. Res. Space Physics*, *120*, 2584–2599, doi:10.1002/2014JA020729.